Quantification of free convection effects on 1 kg mass standards

2015 Metrologia 52 835

(http://iopscience.iop.org/0026-1394/52/6/835)

IOP Publishing | Bureau International des Poids et Mesures Metrologia

Metrologia **52** (2015) 835–841 doi:10.1088/0026-1394/52/6/835

Quantification of free convection effects on 1 kg mass standards

M Schreiber[1], M S Emran[2], T Fröhlich[3], J Schumacher[2] and A Thess[4]

[1] Sartorius Lab Instruments GmbH and Co. KG, D-37075 Göttingen, Germany
[2] Institute of Thermodynamics and Fluid Mechanics, Technische Universität Ilmenau, D-98684 Ilmenau, Germany
[3] Institute of Process Measurement and Sensor Technology, Technische Universität Ilmenau, D-98684 Ilmenau, Germany
[4] Institute of Engineering Thermodynamics, German Aerospace Center (DLR), D-70569 Stuttgart, Germany

E-mail: mario.schreiber@sartorius.com

Received 3 August 2015, revised 16 September 2015
Accepted for publication 21 September 2015
Published 5 November 2015

Abstract

We determine the free-convection effects and the resulting mass differences in a high-precision mass comparator for cylindrical and spherical 1 kg mass standards at different air pressures. The temperature differences are chosen in the millikelvin range and lead to microgram updrafts. Our studies reveal a good agreement between the measurements and direct numerical simulations of the Boussinesq equations of free thermal convection. A higher sensitivity to the free convection effects is found for the spherical case compared to the cylindrical one. We also translate our results on the free convection effects into a form which is used in fluid mechanics: a dimensionless updraft coefficient as a function of the dimensionless Grashof number Gr that quantifies the thermal driving due to temperature differences. This relation displays a unique scaling behavior over nearly four decades in Gr and levels off into geometry-specific constants for the very small Grashof numbers. The obtained results provide a rational framework for estimating systematic errors in mass metrology due to the effects of free convection.

Keywords: convection effects, Boussinesq equations, mass standards, mass metrology

(Some figures may appear in colour only in the online journal)

1. Introduction

The objective of the present work is to investigate and quantify one important source of measurement uncertainty in mass metrology: the effect of convective air flow on the apparent mass of a kilogram standard whose temperature differs from that of the surrounding air. We consider two mass standards with identical mass $m_1 = m_2$ and volume $V_1 = V_2$ as shown in figure 1. The mass standards are placed on a mass comparator balance. We assume that the temperature of one mass standard, T_m, is slightly higher than the temperature of the ambient air, T_∞, i.e. $\Delta T = T_m - T_\infty > 0$. We also assume that the second mass standard has the same temperature as the ambient air, i.e. $\Delta T = T_m - T_\infty = 0$. The temperature difference between the warm body and the ambient air gives rise to free convection in the form of an updraft in the vicinity of the body. The viscous friction between the rising air and the surface of the body creates an upward force F acting on the body. This force is responsible for an apparent mass difference $\Delta m = F/g$ observed between the two mass standards. It should be emphasized that this force has nothing to do with the Archimedian buoyancy force that is excluded from the present consideration by assuming that both bodies which are compared have the same mass and volume.

We will determine the apparent mass difference Δm as a function of the temperature difference ΔT for two different shapes of mass standards, cylindrical and spherical, and for different ambient pressures. We find the determined mass differences to be in good agreement with direct numerical simulations that have been conducted together with the

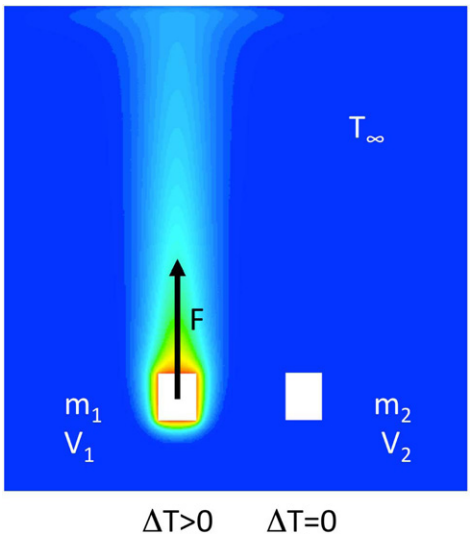

Figure 1. Mass difference due to free convection effects. We show to the left a false colour representation of the steady state temperature distribution as obtained from one of our numerical simulations. The color scale ranges from red for $T_m = 300.6$ K to blue for $T_\infty = 300.0$ K. The pressure was 300 hPa. The full simulation domain around the mass standard extends to 10 times the cylinder diameter in all spatial directions. The constraints are $m_1 = m_2$ and $V_1 = V_2$.

measurements. As being the case in high-precision mass metrology, the temperature difference between the mass and its environment is in the millikelvin range and thus by at least two orders of magnitude smaller than in the previous benchmark experiments by Gläser *et al* [1, 2] and Mana *et al* [3]. Our measurements provide thus more realistic conditions close to thermal equilibrium than the studies conducted in the past. The used mass comparator allows us to quantify the effects under realistic measurement conditions and to achieve a new level of precision.

Several analytical and numerical investigations have been conducted to study free convection around a sphere or a cylindrical body. Among them the numerical solution of a set of two-dimensional asymptotic boundary layer equations by Potter and Riley [4] in the limit of large temperature differences should be mentioned. The temperature differences were given in the non-dimensional Grashof number *Gr*, which is defined as

$$Gr = \frac{g\alpha\Delta T L^3}{\nu^2}, \qquad (1)$$

and relates buoyancy effects to viscous effects in thermal convection. Here, g is the magnitude of the acceleration due to gravity, L the characteristic length of the mass, α the isobaric expansion coefficient and ν the kinematic viscosity of the surrounding air. The characteristic length L is either the height of the cylinder H_c or the diameter of the sphere d_s. An axisymmetric solution for convection around a sphere subject to a sudden temperature increase at the surface has been obtained by Riley [5]. Laminar steady-state convection was reported by Jia and Gogos [6].

Besides the Grashof number, two other dimensionless quantities enter the problem. The Prandtl number $Pr = \nu/\kappa$ relates viscous diffusion which is measured by the kinematic viscosity, ν, to the diffusivity of the temperature field, κ, in the working fluid. The Prandtl number for air is 0.7. The third parameter is the aspect ratio Γ that relates a width (or diameter) to a height in the problem at hand. In our case, $\Gamma = 1$ for the sphere and $\Gamma = d_c/H_c$ for the cylinder with H_c being the height of the cylinder and d_c its diameter.

The outline of the paper is as follows. In section 2 we describe the measurement setup. The section is followed by a short discussion of the numerical simulations. Section 4 presents the results and a discussion.

2. Measurement setup

For the experimental determination of the mass difference of two mass standards the temperature is ideally zero or practically in the range of a few mK. In Gläser [1] stainless steel 1 kg mass standards of cylindrical shape are explored with much higher temperature differences. The reason is that it is not possible to use a contact temperature sensor during the weighing because of the disturbing force. Contactless temperature sensors cannot provide the required sub-millikelvin accuracy. We measured at temperature differences less than 60 mK yielding small changes of the mass difference of only some µg per 1 kg nominal mass. For this we used a modified CCL1007 mass comparator (see figure 2(a)) with an automated load alternator inside an air-tight vacuum chamber [7]. The load alternator has eight positions for cylindrical or spherical mass standards, lifts the weights from the moving table and moves them down to the balance pan for weighing. We mounted a temperature sensor above the weighing pan position to get in mechanical contact with the top surface of the weight during the movement of the mass standards to the pan and back to the moving table (see figure 2(b)). This works for cylindrical or spherical mass standards of different heights because we are able to adjust the vertical position of the temperature sensor. The temperature sensor is a Pt-10 000 resistance thermometer with a special holder made of PEEK plastics to thermally isolate the back of the sensor from the surrounding air temperature (see figure 2(c)). We corrected the readings of the temperature sensor for self heating and thermal contact resistance. We compared the reading of the contact Pt-10 000 resistance thermometer with a sensor located in the center of a modified mass standard with heat-conductive paste. After the correction the offset temperature is less than 2 mK.

The vacuum chamber of the CCL1007 mass comparator allows to take measurements under air tight conditions. We made our mass comparisons under 300 hPa, 600 hPa and 960 hPa which is the usual pressure in our lab because we are about 550 m above sea level. After evacuation to the desired pressure level the setup relaxed 24 h to thermal equilibrium. This means all mechanical parts, the air inside the chamber and all mass standards have the same temperature with differences less than 1 mK. We use two pairs of mass standards of the same shape, size and nearly the same mass: a pair of stainless steel cylinders ($d_c = 50.5$ mm $H_c = 63.85$ mm) and two single crystal silicon spheres ($d_s = 93.6$ mm) for the mass comparisons. One of the mass standards was heated by about

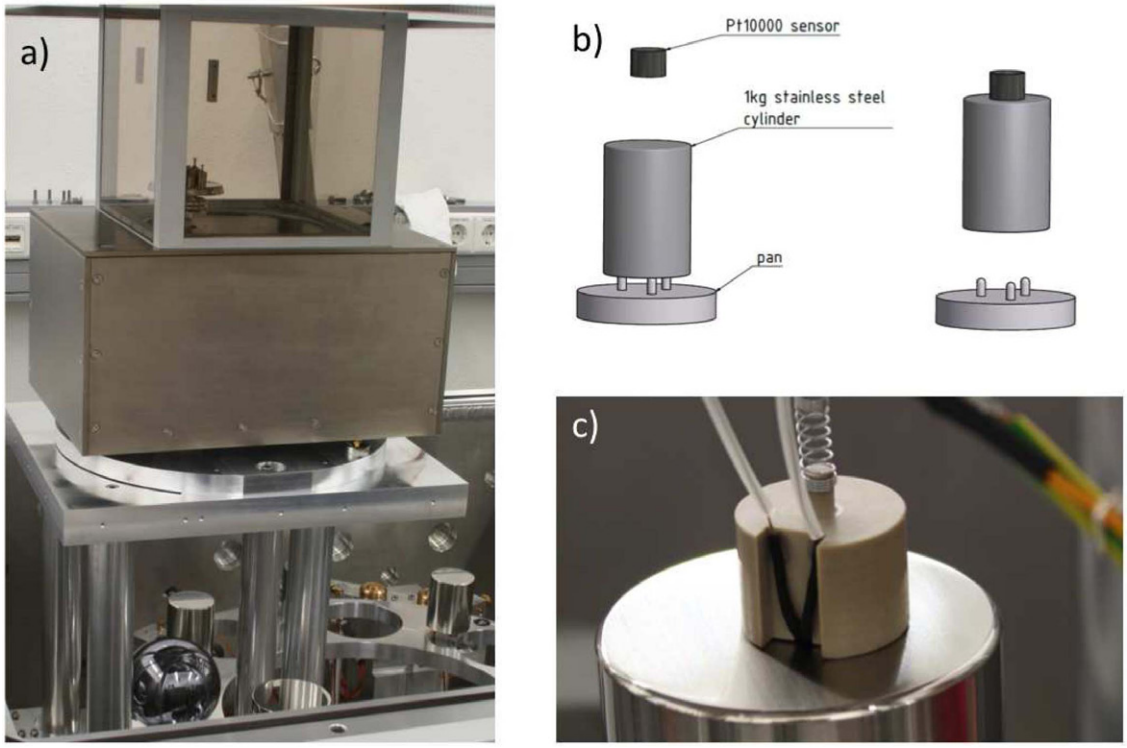

Figure 2. Experimental setup. (a) Interior of the comparator mass balance with the spherical mass standard. (b) The cylindrical 1 kg mass standard during weighing (left) and during temperature measurement (right). (c) Temperature sensor in contact with the upper surface of the cylinder.

40 … 60 mK using a green 100 mW diode laser through a glass window in the vacuum chamber before the measurement was started. The second mass standard of the same material and shape resting on a different position of the load alternator of the mass comparator still has the same temperature as the air and all other parts. It is used as a reference for the temperature measurement and for the mass determination.

With this set-up we can measure the temperature difference between the two masses with sub-mK repeatability always between the loadings of the mass standards to the mass comparator pan. For the determination of the current mass difference Δm we use the typical ABBA scheme [12] and look for the change Δm of this mass difference compared to the mass difference after thermal equilibrium.

To double check the results we changed the heated mass standard in the ABBA scheme. The results of both measurements are found to agree.

3. Numerical simulations

We solve the Boussinesq equations for the velocity, u_i, the temperature, T, and the pressure, p which are given by [8]

$$\frac{\partial u_j}{\partial x_j} = 0, \tag{2}$$

$$\frac{\partial u_i}{\partial t} + u_j \frac{\partial u_i}{\partial x_j} = -\frac{1}{\rho_\infty}\frac{\partial p}{\partial x_i} + \nu \frac{\partial^2 u_i}{\partial x_j^2} + g\alpha(T - T_\infty)\delta_{i3}, \tag{3}$$

$$\frac{\partial T}{\partial t} + u_j \frac{\partial T}{\partial x_j} = \kappa \frac{\partial^2 T}{\partial x_j^2}, \tag{4}$$

with $i, j = x, y, z$ and the Kronecker symbol δ_{ij}. Summation is done with respect to j in (2)–(4). The parameter κ is the thermal diffusivity of the temperature field and ρ_∞ is the reference mass density. Buoyancy effects enter (3) for the vertical velocity component only and thus couple the velocity and temperature fields. In the Boussinesq approximation, it is assumed that the temperature dependence of the mass density of the fluid enters the buoyancy term only (see also the review by Chillà and Schumacher [9]).

The simulations are carried out in the half space which results in a computational domain of $V = \{(r, \phi, \theta \mid 0 \leqslant r \leqslant 20 d_s),\ 0 \leqslant \phi, \theta \leqslant \pi\}$ for the spherical geometry. The computational domain of the cylindrical case is defined correspondingly. We apply a finite volume method implemented in the commercial software package ANSYS Fluent [10] without any turbulence model. The grid is strongly refined towards the masses such that the fine boundary layers are resolved. The computational domain for the cylinder case is covered by 11.3 million mesh cells, the one for the spherical case by 2.3 million mesh elements such that all relevant fluid scales are resolved. The surface of the mass is kept at a constant temperature T_m, the outer boundary at T_∞. No-slip boundary conditions for the velocity field hold at the mass, free-slip boundary conditions at the outer walls. A typical steady temperature distribution is shown in figure 1 which would correspond with $Gr = 1690$. We observe the formation of a thin thermal boundary layer around the cylinder which

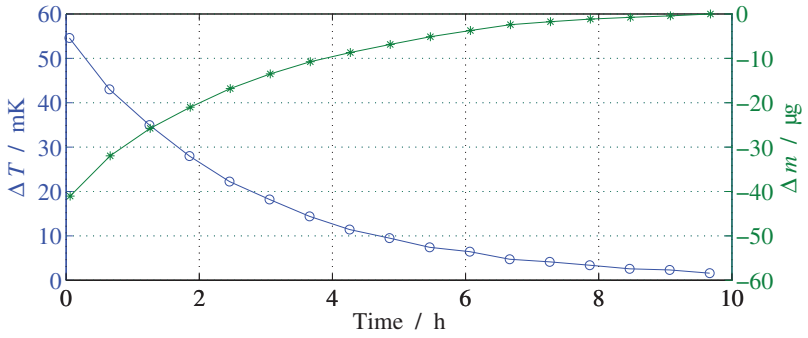

Figure 3. Temperature difference (circles) between two cylindrical 1 kg mass standards and the change of the mass difference (asterisks) over time in hours after laser heating one of masses to 60 mK over temperature.

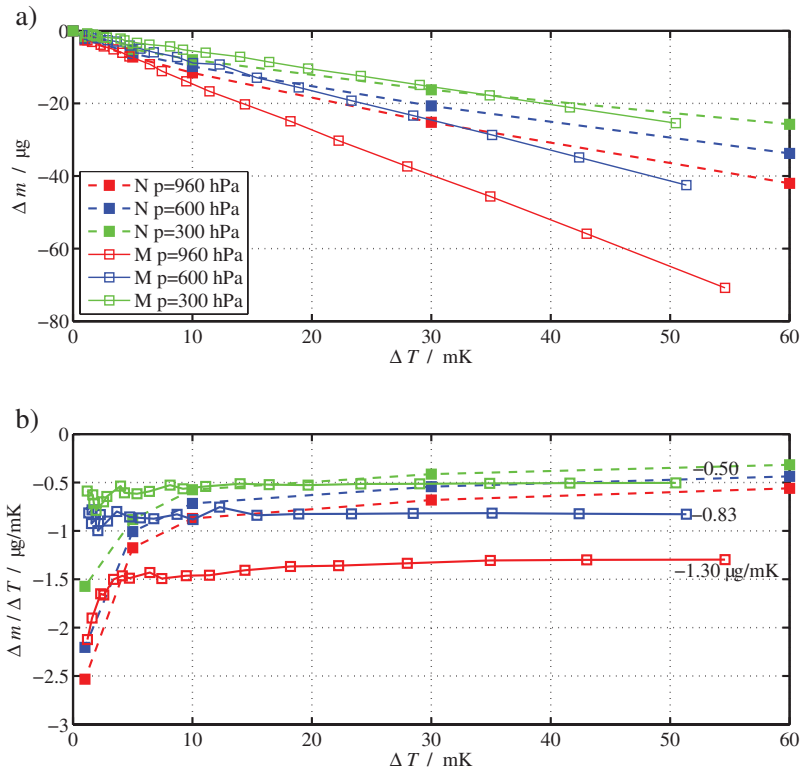

Figure 4. Cylindrical 1 kg mass standards; results for numerical simulations (N) and measurement (M). Mass differences are corrected for buoyancy. (a) Change of mass difference in µg as a function of temperature difference in mK. (b) Sensitivity β of mass change per temperature in µg mK^{-1}as a function of temperature difference in mK. The sensitivity would correspond to a derivative with respect to the temperature for the limit $\Delta T \to 0$.

converges into a cusp-like pattern above the cylinder. The velocity and temperature fields for the small temperature differences are always stationary.

4. Results and discussion

The slow cooling of the first mass standard in the experiment gives us time to determine mass and temperature differences between the loadings. Figure 3 shows the change of the temperature difference ΔT between the two mass standards and the change Δm of the mass difference for the stainless steel 1 kg mass standards at 960 hPa air pressure. The temperature difference starts with 54.6 mK causing an apparent mass difference of −41.3 µg. This implies that the heated mass standard seems to be lighter. In the measurement, the apparent mass difference is the sum of the fluid mechanical updraft and the air buoyancy change due to a change of air density and thermal volume expansion of the mass standard material. We calculate the fluid mechanical updraft in the simulation and can consequently correct the measured values by subtracting the calculated buoyancy contribution which is 27.9 µg in the example above giving a difference of −69.2 µg caused by the fluid mechanical updraft. The relation

$$\Delta m(t) = m(t) - m(\infty) - m_0\left[\frac{\varrho_{\mathrm{air}}(20\,^{\circ}\mathrm{C})}{\varrho_{\mathrm{m}}} - \frac{\varrho_{\mathrm{air}}(20\,^{\circ}\mathrm{C}+\Delta T)}{\varrho_{\mathrm{m}}(1+\gamma\Delta T)}\right] \quad (5)$$

is used to correct all balance readings for the buoyancy contribution. The air density ϱ_{air} is calculated using the formula

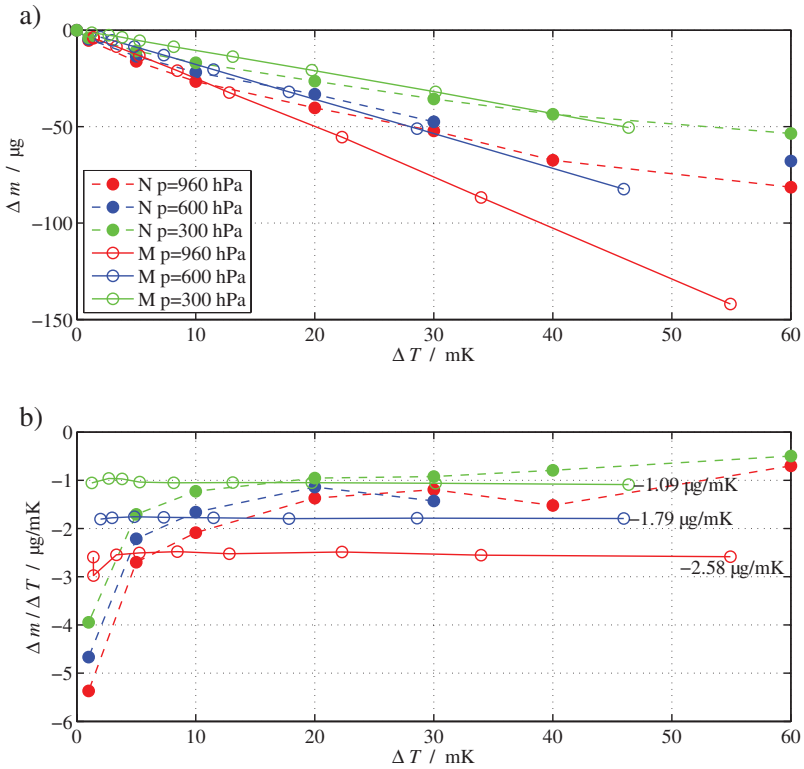

Figure 5. Spherical 1 kg mass standards; results for numerical simulations (N) and measurement (M). Mass differences are corrected for buoyancy. (a) Change of mass difference in µg as a function of temperature difference in mK. (b) Sensitivity β of mass change per temperature in µg mK^{-1} as a function of temperature difference in mK.

[12] of the International Committee of Weights and Measures. The density ϱ_m of the mass standard is known and the volume expansion coefficient γ is taken from the literature.

Figure 4 compares measurement and simulation for the cylindrical mass at three different pressures. We display the change of the mass difference, Δm, versus the temperature difference, ΔT, in panel (a) and a compensated plot in panel (b) to highlight the sensitivity. The sensitivity is given by

$$\beta(\Delta T) = \frac{\Delta m}{\Delta T} = \frac{F}{g\Delta T}, \qquad (6)$$

where F is the total updraft force. Closed symbols are for the simulations (N) and open symbols for the measurements (M). For the lowest pressure, the numerical prediction is in good agreement with the measurement. For the highest pressure the deviations become larger. Furthermore, deviations of the sensitivity in figure 4(b) are found particularly for the smallest temperature differences below $\Delta T = 10$ mK. Here, the simulations, which we kept in a time-dependent integration scheme, advance very slowly and the measurement of the relation between Δm and ΔT is most challenging in terms of the accuracy. In figure 5, the comparison is repeated for the spherical mass standard. The conclusions which can be drawn agree with those of the cylindrical case. The mean slopes of the sensitivity, $\overline{\beta}$, are summarized in table 1 and compared with [3] and [11]. They increase with increasing pressure in both cases reflecting the enhanced air mass density and thus the enhanced friction forces. In agreement with Mana *et al* [3], the sensitivity for the sphere is larger than for the cylinder

Table 1. Results for the mean sensitivity $\overline{\beta}$ (see also equation (6)) in µg mK^{-1} at different pressures and for $\Delta T = 60$ mK compared to experimental results at lab pressure given by Gläser [11] in table 4 applied at $\Delta T = 60$ mK and in table 2 of Mana *et al* [3] for $\Delta T = 200$ mK.

	Measurement		Simulation	
Pressure	Sphere	Cylinder	Sphere	Cylinder
300 hPa	−1.09	−0.50	−0.89	−0.43
600 hPa	−1.79	−0.83	−1.13	−0.56
960 hPa	−2.58	−1.30	−1.36	−0.70
Gläser [11]		−0.51		
Mana *et al* [3]	−0.52	−0.37	−0.43	−0.36

Note: The surface area for the sphere is $A_O = 27\,523$ mm^2, for the cylinder $A_O = 14\,136$ mm^2.

although the magnitudes differ. In the case of the sphere, we observe a gradually growing boundary layer in our simulations starting from the bottom of the equally curved surface. The situation is different for the cylinder. The lower edge of the cylinder mass standard, which is from the hydrodynamic perspective a singularity, will suppress the formation of a gradually growing boundary layer as seen in figure 1. This can be a reason for the reduced sensitivity $\beta(\Delta T)$ in the cylindrical case. Consequently, a comparison of cylindrical mass standards at different aspect ratios would be a next step to refine this analysis. These efforts are currently in progress.

How is this sensitivity β translated into a fluid mechanics perspective? The updraft force can be estimated by the drag which is generated due to the initialized motion. For very

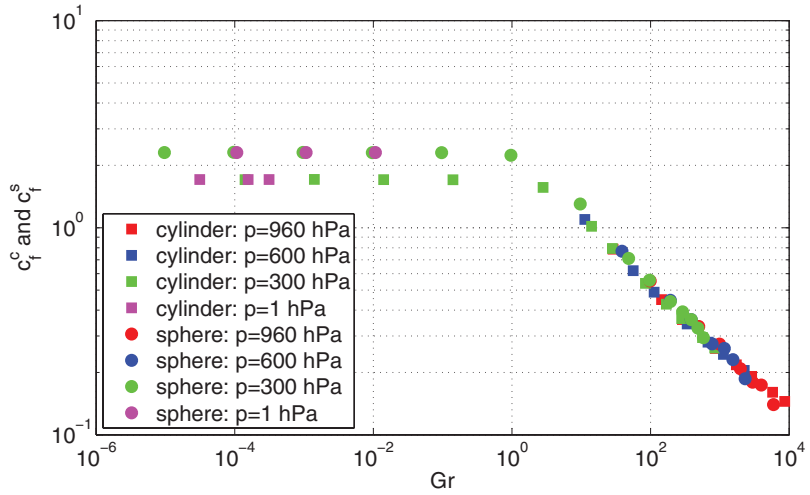

Figure 6. Updraft coefficients for the cylinder and the sphere versus the Grashof number. We show the data for different air pressures. All updraft coefficients in this figure have been obtained from numerical simulations (see legend).

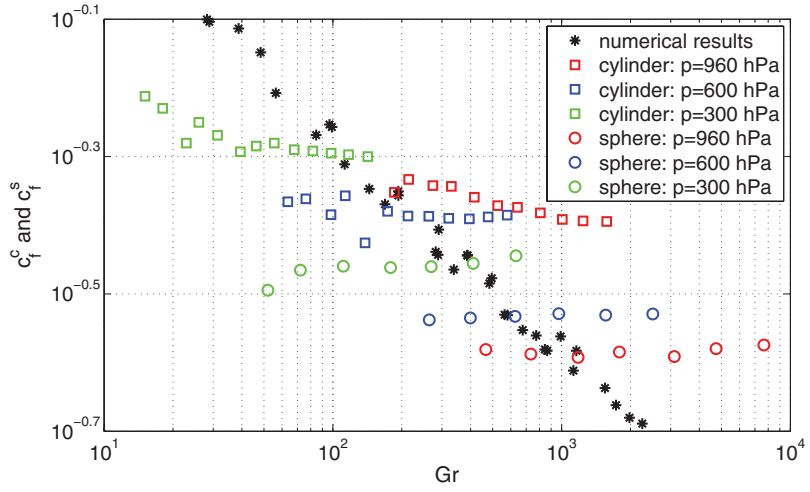

Figure 7. Comparison of the updraft coefficients for the measurement and simulation. We show the range of Grashof numbers only that is accessible for both simulation and experiment (compare also with figure 6). Closed symbols are for the simulations and open symbols for the experiments.

small ΔT, we can assume an equilibrium between the buoyancy term and the viscous forces in (3), i.e. $\alpha g \Delta T \sim \nu v / L^2$ where v is a typical velocity magnitude. The Stokes drag force $F \sim \varrho_{\mathrm{air}} \nu v L$ translates then into $F \sim \varrho_{\mathrm{air}} \alpha g \Delta T L^3$.

For larger temperature differences, one assumes an equilibrium between buoyancy and fluid inertia effects, i.e. $\alpha g \Delta T \sim v^2 / L$. The drag force is $F \sim \varrho_{\mathrm{air}} v^2 L^2$ and thus again $F \sim \varrho_{\mathrm{air}} \alpha g \Delta T L^3$. Both expressions are the same and thus the updraft force can be set to

$$F = c_{\mathrm{f}}(Gr, Pr, \Gamma) \varrho_{\mathrm{air}} \alpha g \Delta T A_{\mathrm{O}}, \tag{7}$$

where A_{O} is the surface of the mass standard.

The dimensionless *updraft coefficient* c_{f} in (7) contains now the dependence on the Grashof and Prandtl numbers as well as the aspect ratio. Here, neither the Prandtl number nor the aspect ratio are varied. With $L = d_{\mathrm{s}}$ for the sphere and $L = H_{\mathrm{c}}$ for the cylinder we obtain the following expressions for the sphere (s) and the cylinder (c) by a combination of equations (6) and (7)

$$c_{\mathrm{f}}^{\mathrm{s}}(Gr) = \frac{\beta^{\mathrm{s}}}{\pi \varrho_{\mathrm{air}} \alpha d_{\mathrm{s}}^3}, \tag{8}$$

$$c_{\mathrm{f}}^{\mathrm{c}}(Gr) = \frac{\beta^{\mathrm{c}}}{\pi \varrho_{\mathrm{air}} \alpha H_{\mathrm{c}}^3 (\Gamma^2/2 + \Gamma)}. \tag{9}$$

The aspect ratio $\Gamma = 0.791$ has to be used for the cylindrical mass standard. In figure 6, we plot both coefficients c_{f} versus Gr. We observe that the data points for different pressures, but the same geometry, fall onto each other. For the smallest Grashof numbers, the updraft coefficients level off to a constant value that depends on the particular geometry of the mass standard. Since the boundary layer formation is affected by the edge in the cylindrical case, we can expect that the asymptotic values for very small Grashof numbers will differ in comparison to the sphere. In this regime, the updraft force is directly proportional to the tiny temperature difference.

In figure 7, we replot the numerical simulation data and add the measurements for the range of Grashof numbers

that is accessible in the laboratory experiments. The measurements are found to group around the numerical simulation data. We observe furthermore that the series are also almost constant. Deviations which were detected already in figures 4 and 5 are present again in this plot. Two reasons can be given for this result: First, we note that the range of Grashof numbers which can be accessed in the experiment is limited since temperature differences below 1 mK cannot be measured in the laboratory. Secondly, the simulations considered the mass standards only and neglected parts that hold the standards, balance pan, lifting device and other surrounding parts. These parts would affect the boundary layer formation around the standards and the resulting force and thus enhance the complexity of the numerical investigations significantly. Such simulations are not possible with the given resources. We wish to stress, however, that experimental and numerical results fall consistently into the same range which is a significant step forward given the very small temperature difference to which the whole study was limited.

In summary, we have quantified the free convection effects and the resulting mass differences which arise due to temperature differences between the mass standard and its environment. Our study in the millikelvin range with direct measurement of the temperature differences reveals a linear dependency of the apparent mass over the temperature with a higher sensitivity than given by previous studies. Furthermore, our experimental results show that the sensitivity is linearly dependent on the air density. When translated into a fluid mechanical framework our results reveal a universal scaling behavior for a dimensionless updraft coefficient c_f (which is defined similarly to a drag coefficient) versus the Grashof number Gr. In the limit of very small Gr (or temperature differences) this updraft coefficient is found to level off to a constant value that depends on the geometry of the mass standard. Note also that (at least in the simulations) the data points for different air pressures in the chamber fall onto each other very well.

As a next step, it would be interesting, in our view, to extend this study to cylindrical mass standards of different aspect ratios in order to obtain a more comprehensive picture of the asymptotic behavior at very small Grashof numbers. Our results demonstrate clearly that for a stainless steel cylinder and silicon sphere 1 kg mass standards the effects of temperature induced fluid mechanical updrafts can be quantified as systematic errors under conditions of high-precision mass metrology.

Acknowledgments

The authors gratefully acknowledge financial support from the Deutsche Forschungsgemeinschaft in the framework of the Research Training Group 1567 ‘Lorentz force velocimetry and Lorentz force eddy current testing’.

References

[1] Gläser M 1990 *Metrologia* **27** 95–100
[2] Gläser M and Do J Y 1993 *Metrologia* **39** 67–73
[3] Mana G, Palmisano C, Perosino A, Pettorruso S, Peuto A and Zosi G 2002 *Meas. Sci. Technol.* **13** 13–20
[4] Potter J M and Riley N 1980 *J. Fluid Mech.* **100** 769–83
[5] Riley N 1986 *Comput. Fluids* **14** 225–37
[6] Jia H and Gogos G 1996 *Int. J. Heat Mass Transfer* **39** 1603–15
[7] Borys M, Fehling T, Fröhlich T, Heydenbluth D, Mecke M and Schwartz R 2006 *Proc. of 18 IMEKO World Congress (Rio de Janeiro)* pp 176.1–.5
[8] Tritton D J 1988 *Physical Fluid Dynamics* (Oxford: Clarendon)
[9] Chillà F and Schumacher J 2012 *Eur. J. Phys.* E **35** 58
[10] ANSYS Fluent, Version 14, 2013 www.ansys.com
[11] Gläser M 1999 *Metrologia* **36** 183–97
[12] Edition 2004 Recommendation No. 111 www.oiml.org